Transactions **of the SMiRT 27**
Yokohama, Japan, March 3-8, 2024
Division V

STUDY ON SEISMIC SSI EFFECTS FOR DEEPLY EMBEDDED BASE-ISOLATED SMR ON DIFFERENT SITE CONDITIONS

Dan M. Ghiocel[1], Kyung Lee[2], Daniel Lemley[2], Branko Galunic[2],
Enver Odar[3], Bob Iotti[3]

[1] Ghiocel Predictive Technologies, Inc., Pittsford, New York, US (dan.ghiocel@ghiocel-tech.com)
[2] United Engineers & Constructors, Mt. Laurel, New Jersey, US
[3] ARC Clean Energy, Washington, D.C., USA

ABSTRACT

The paper presents results of a research study which addresses the seismic SSI analysis of a deeply embedded base-isolated SMR structure. The seismic SSI study includes three generic site-specific conditions with severe 0.50g seismic ground surface acceleration inputs. The investigated ARC-100 SMR design includes a base-isolation system consisting of Friction Pendulum (FP) isolators. A multistep seismic SSI methodology as recommended in the ASCE 4-16 Chapter 12 is applied.

Two base-isolation design solutions were investigated: 1) Option 1, including two base-level isolation system, and 2) Option 2, including a single base-level isolation system. The paper shows that for Option 1, basically, the isolated superstructure behaves as a multiple supported nonlinear dynamic system excited by the slightly different isolator support motion inputs. To avoid unnecessary analysis complexities for the base-isolated SMR, beyond the ASCE 4-16 and ASCE 7-22 guidelines, the Option 2 with a single base-isolation level was finally selected as more robust base-isolation design solution. The Option 2 has a simpler base-isolation system which can be accurately analysed based on the SIDRS concept in compliance with the ASCE 4-16 standard and the most NRC regulatory recommendations.

This research paper focuses on the Step 1 seismic SSI analysis behaviour of the isolated SMR Option 1 with two base-isolation levels, and provides unique practical insights for this multilevel base-isolation solution behaviour, as a lesson learned during the process of optimizing the base-isolated ARC-100 SMR design.

1. SEISMIC METHODOLOGY

A two-step seismic SSI methodology as recommended in the ASCE 4-16 Chapter 12 is applied. The two-step seismic SSI methodology includes:

1) *Step 1*, perform overall seismic SSI analysis using an efficient hybrid frequency-time approach that directly computes the converged iterated-properties of the equivalent-linear hysteretic isolators and determine the SSI foundation motion (isolator pedestal support motions), and

2) *Step 2*, perform a nonlinear dynamic analysis of the superstructure in time-domain including refined nonlinear models of the hysteretic base-isolators subjected to the SSI motions computed at the isolator pedestal supports.

The ACS SASSI Option NON software was used for Step 1, and the SAP2000 software was used for Step 2. SAP2000 includes a detailed friction pendulum nonlinear modelling in time-domain.

The concept of the two-step seismic SSI analysis is illustrated in Figure 1. In this paper, the Step 1 seismic SSI analysis results are discussed in detail for the two base-isolation level SMR design. The single base-isolation level SMR design results will be addressed in a separate paper.

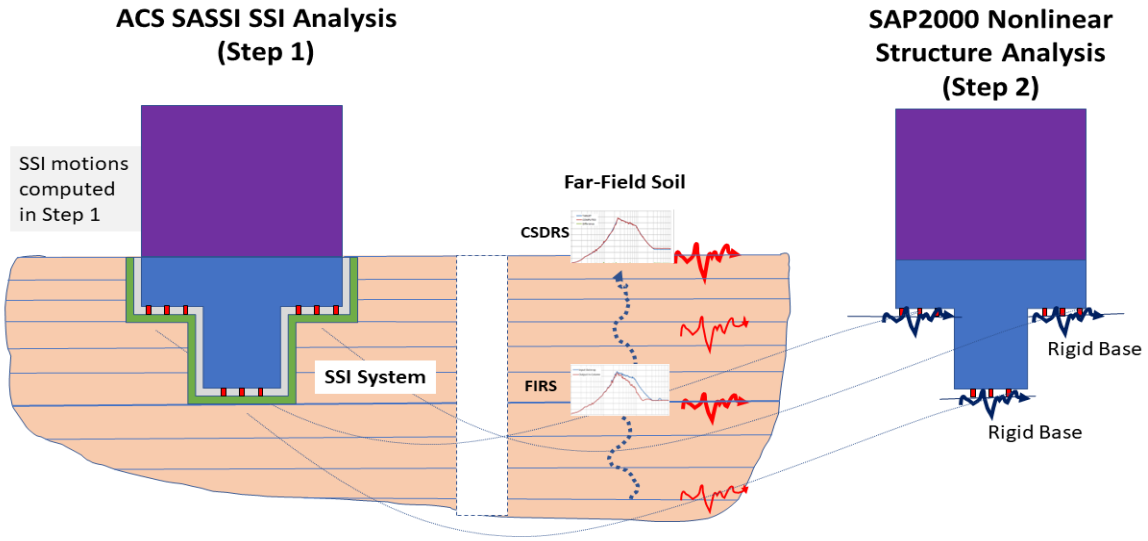

Figure 1. Two-Step Seismic SSI Analysis Applied to Deeply Embedded Base-Isolated ARC-100 SMR

The two investigated base-isolation design solutions considered in the research study are sketched in Figure 2: 1) Option 1, Initial solution including two base levels with FP isolators, and 2) Option 2, Final optimized solution including a single base level with FP isolators.

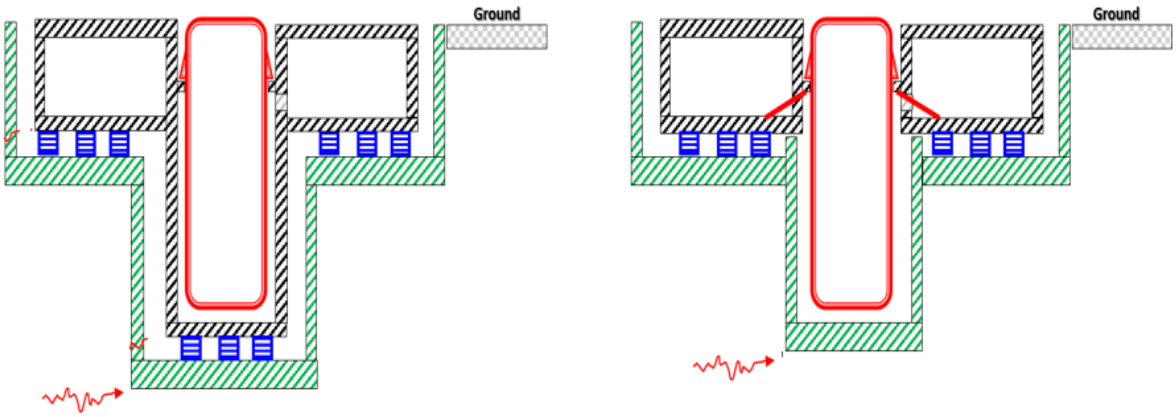

Figure 2: Base-Isolated Embedment ARC-100 SMR Design Option 1 (left) and Option 2 (right)

Only the seismic SSI analysis results obtained for the Option 1 design solution are included herein.

2. GENERIC SITE CONDITIONS FOR SEISMIC SSI ANALYSIS

The seismic SSI analysis of the base-isolated ARC-100 SMR structure was performed for selected generic site-specific conditions covering a large range of geological and seismological site conditions, from firm soils to hard-rock sites.

The three generic site soil profiles were combined with two seismic CSDRS inputs specific to each soil type, as shown in Figure 3.

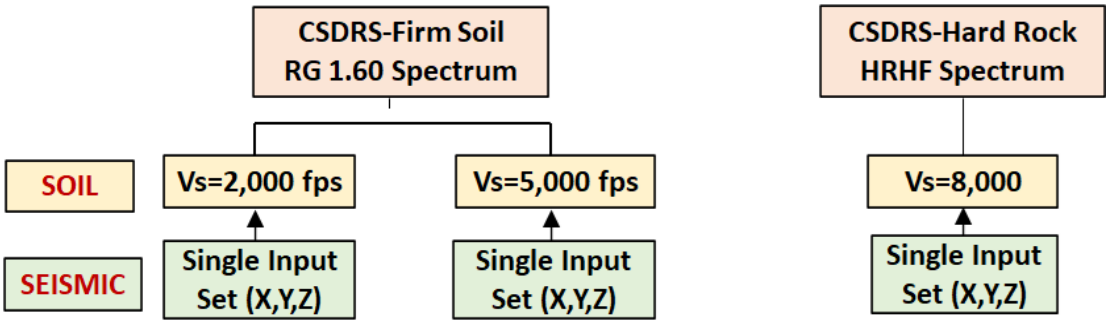

Figure 3. Generic Site-Specific Conditions for the ARC-100 SMR Conceptual Design Research Study

The CSDRS shapes for the two generic soil sites are exactly the RG1.60 spectrum shape, while the CSDRS-HF (High-Frequency) shape for the hard-rock site follows closely the Seabrook site-specific spectrum shape. The CSDRS inputs plotted in Figure 4 were applied to both horizontal and vertical directions. It should be noted that for this preliminary research study, only a single input set of spectrum compatible acceleration time histories was considered for each soil type (not compliant with the multiple input set requirements in ASCE 4-16 Section 12 and ASCE 7-22 Section 17 for isolated structure design).

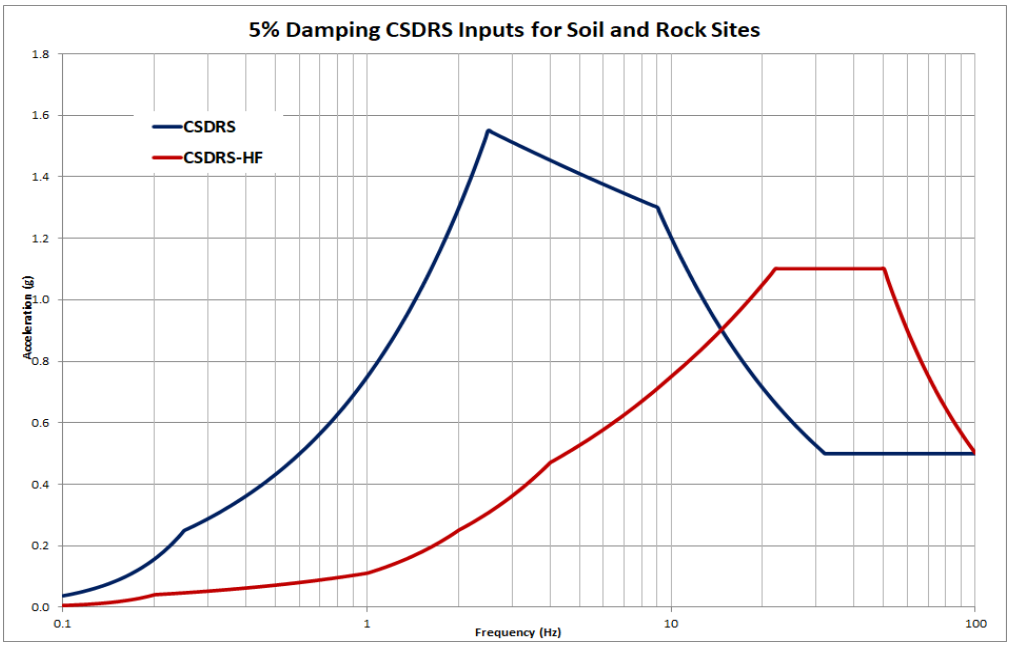

Figure 4. Two CSDRS Inputs Were Considered for the ARC-100 RB Conceptual Design Study

Two seismic input sets of spectrum compatible acceleration time histories were generated for: 1) Firm Soil CSDRS (with RG1.60 spectrum shape) and 2) Hard Rock CSDRS-HF (with Seabrook site spectrum shape). The two sets of seismic input accelerations were generated per the NRC SRP 3.7.1 requirements for the Option 1, Approach 2. In addition to the NRC SRP 3.7.1 requirements of Option 1, Approach 2, as recommended by Nie in the NRC RIL-2019 report (Nie et al., 2019), the strong motion interval PSD of the generated accelerations were checked against the target minimum PSDs. to ensure that there is no frequency content deficiency for the generated time histories.

The FP isolator sliding mode frequency were expected to be @ 0.30 Hz for the soil sites and @ 1.25 Hz for the hard-rock site based on the ASCE 7-22 Chapter 17 equations.

The CSDRS compatible acceleration time histories were generated using the ACS SASSI EQUAKE module which includes a refined frequency-time acceleration baseline correction algorithm for accurate computation of the velocity and displacement time histories. The EQUAKE module uses the Fourier spectrum zero-padding acceleration interpolation recommended by ASCE 43-19 for computing ARS in the high-frequency range.

3. DEEPLY EMBEDDED BASE-ISOLATED ARC-100 SMR MODEL FOR OPTION 1

The embedded ARC-100 SMR structure has a total height above ground level of 75 ft and an embedment of 76 ft depth, as shown in Figure 5. The moat foundation is a cylindrical wall with two base levels. The moat wall at the top horizontal diameter at the upper-base level is 124 ft. Figure 5 shows the base-isolated ARC-100 SMR structure ANSYS model. This ANSYS model is for Option 1 with FP isolators distributed at two base-isolation levels, including 24 FP isolators at the upper-level and 6 isolators at the lower-level.

The ANSYS structure model was automatically converted using ACS SASSI UI into a complete SASSI type model, including both the SMR structure model, the excavated soil model and the far-field soil layering. The FP isolators were modelled by nonlinear spring elements in the SSI model, while the pedestal blocks supporting the isolators were modelled by very stiff beam elements plotted in green colour. The moat foundation including the two base-isolation levels, the upper level (UL) and lower level (LL), and the embedded stepped wall is plotted in the yellow colour.

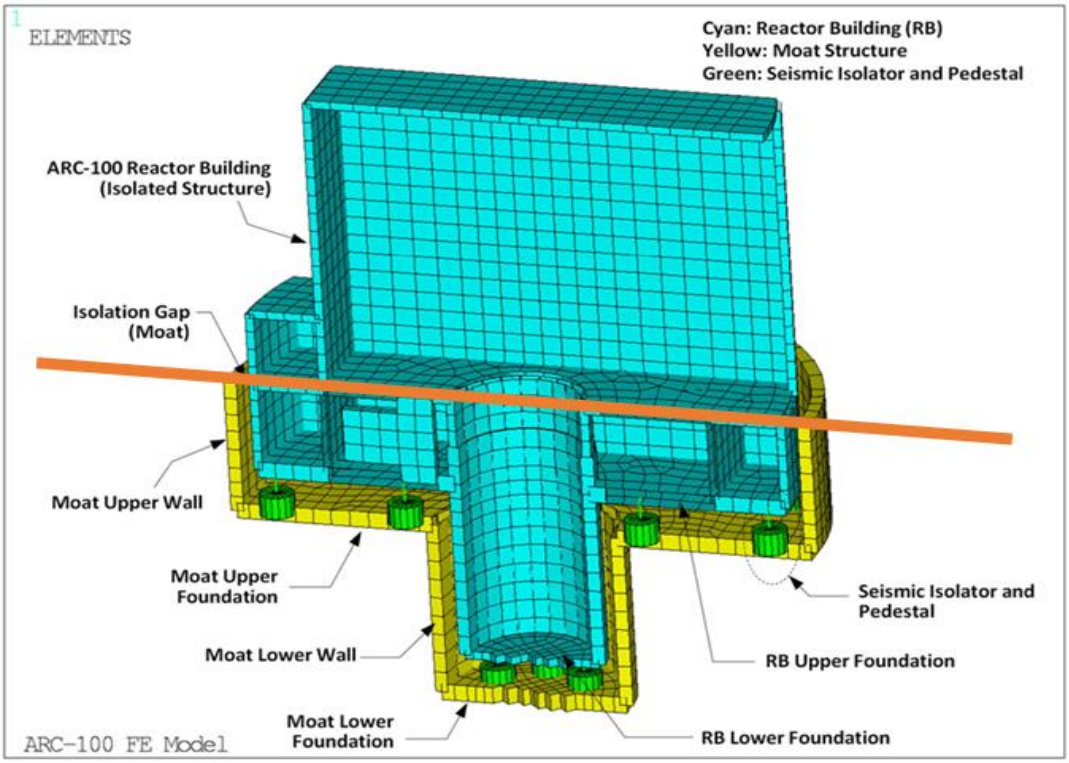

Figure 5. Deeply Embedded Base-Isolated ARC-100 SMR Structure ANSYS FE Model

Figure 6 shows the distribution of the FP isolators on the two moat foundation base slabs at the Upper Level (UL) and Lower Level (LL). There are three FP isolator types with a total number of 30 isolators at the two base levels; there are six Type 1 isolators for LL, and 14 Type 2 and 10 Type 3 isolators for UL. The three types of FP isolators distributed at the two base levels were selected based on the isolator axial load due to gravity.

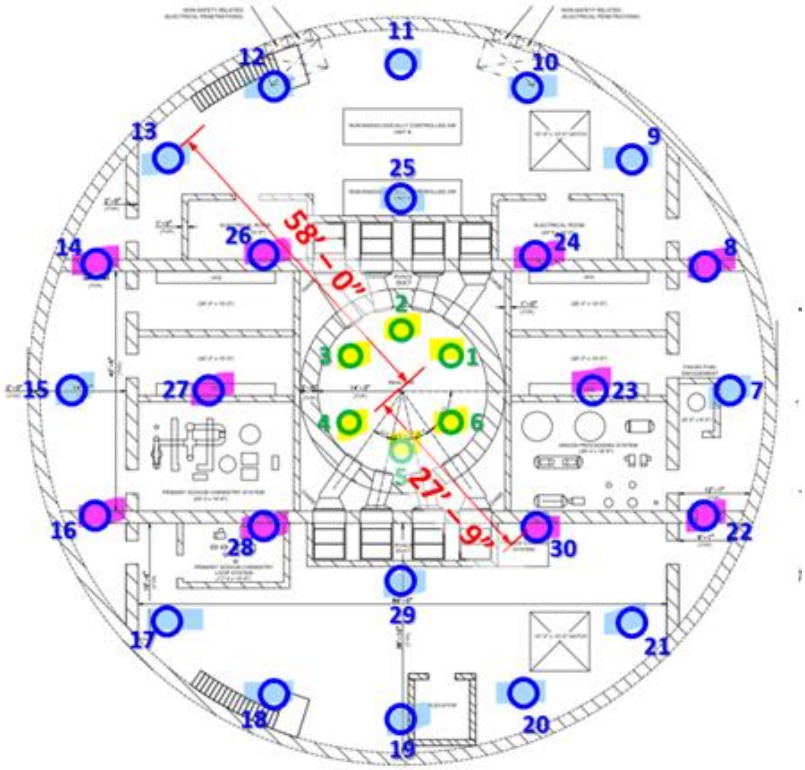

Figure 6: ARC-100 SMR FP Isolator Distribution at the Two Base-Isolation Levels (UL and LL)

The nonlinear modelling of FP isolators requires the computation of the back-borne curve (BBC) for each isolator as a function of their geometry configurations and vertical loads. In addition, an appropriate hysteretic model for the FP isolator behaviour should be considered. Per the ASCE 7-22 Chapter 17, the FP isolators should be modelled by bilinear hysteretic models.

The back-bone curves (BBC) of the FP isolators were analytically computed. The FP isolator has a force-displacement relationship in the horizontal direction at high speed motion is computed as a function of the isolator parameters, W, the compressive vertical gravity load on the isolator, Reff is the effective radius of curvature and F_f the isolator friction force given by $F_f = \mu W$, where μ is the coefficient of friction at the sliding interface at large velocity of sliding. The friction force corresponds to the "yielding" point in the FP isolator BBC. In the vertical direction, the FP isolators have a linear behaviour with a large stiffness; 100,000 kips/in for the Type 1 and 2 FP isolators, and 200,000 kips/in for Type 3 FP isolators. The computed 30 isolator BBC including the three isolator types are plotted in Figure 7.

It should be noted that for seismic SSI analysis per the ASCE 7-22 equation 17-8-1, the equivalent-linear isolator stiffness should be computed based on the maximum values of the FP isolator relative shear displacement and forces. Further, the ASCE 7-22 provides equations to compute these maximum values of the isolator displacements and forces, but these values are obtained without including the SSI effects.

To capture the FP isolator hysteretic behaviour including the seismic SSI effects, the ACS SASSI Option NON uses an iterative equivalent-linearization procedure in Step 1 which couples two analysis substeps: 1) Substep 1 includes *the equivalent-linear SASSI analysis* in complex frequency domain for computing the FP isolator sliding displacements, and 2) Substep 2 includes *the nonlinear hysteretic analyses* in time-domain for computing the isolator nonlinear shear forces given the iterated sliding displacements for each FP isolator assuming a bilinear hysteretic behaviour.

The bilinear hysteretic model for FP isolator called the "General Massing Rule (GMR)" model (Model 4 from the Option NON hysteretic model library list) was applied. Based on the computed isolator

displacements and nonlinear forces in Step 2, the FP isolator effective or equivalent-linear stiffnesses were iteratively computed as Keff = f (Dm, Fm), where Dm and Fm are the iterated maximum values of the isolator sliding displacements and nonlinear forces, respectively.

Per the recent draft of the coming ASCE 4 standard Section 12 (dated by 8/20/2021) *"Multiple calculations may have to be performed to ensure the assumed linear properties of the isolators, which depend on isolator displacement, are reasonable. The equivalent linear properties of the isolators should be recalculated after an analysis and compared with the assumed properties. An update of the numerical model is unnecessary if the difference between assumed and calculated equivalent stiffness and equivalent viscous damping ratio for the isolators and dampers is less than or equal to 15%."*

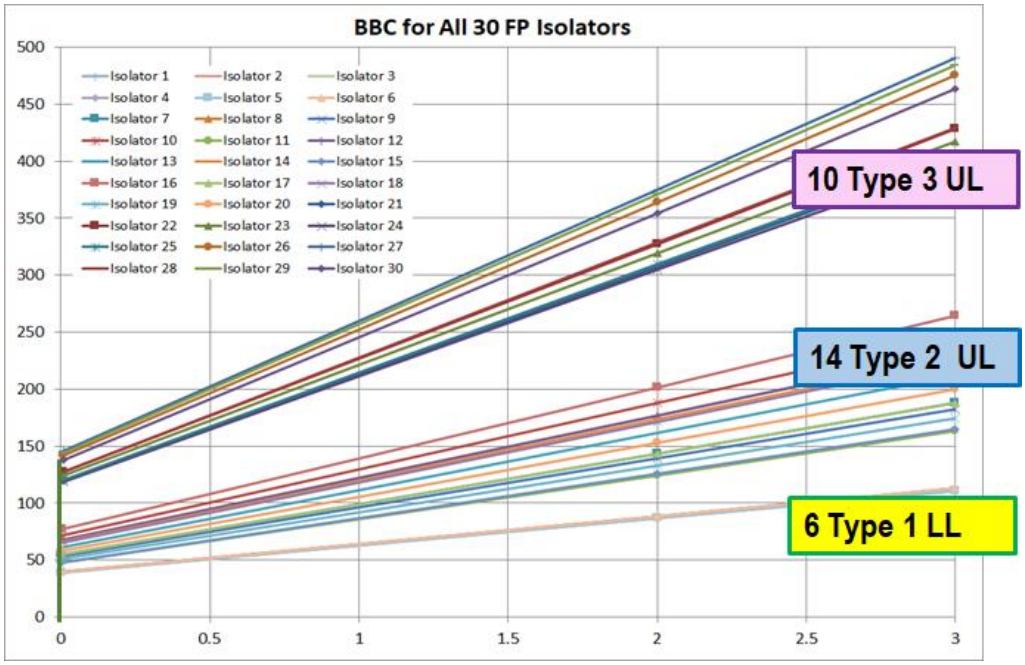

Figure 7. Computed BBC for the 30 ARC-100 FP Isolators of Three Different Types

The iterative SSI analysis procedure in Step 1 converged in 3-4 iterations, as shown in Figure 8 for the UL Type 2 FP isolators for the Vs = 2,000 fps soil case. Since the equivalent-linear modelling is based on the BBC computed based only on the gravity static loads, any potential uplift or cliff-jump nonlinear effects for the FP isolators can't be captured in Step 1, but only in Step 2.

4. DEEPLY EMBEDDER BASE-ISOLATED SMR SSI ANALYSIS RESULTS

To check firstly the accuracy of the equivalent-linear modelling of the FP isolators, the iterated equivalent-linear isolator stiffnesses were averaged for each of the two bases levels and compared with the average equivalent-linear isolator stiffness computed using ASCE 7-22 Chapter 17 equations, as shown in Table 1. The percent differences between the computed equivalent stiffnesses by the SSI analysis and by the ASCE 7-22 Chapter 17 equations were well below the standard required 15% difference.

A final comparison of the iterative equivalent-linearization modelling of the FP isolators for SSI analysis was done after the SAP2000 isolated-superstructure nonlinear analyses were completed. In comparison with the ACS SASSI SSI analysis FP isolator relative displacement of 16.2 in for Vs=2,000 fps soil case, the computed SAP2000 maximum nonlinear isolator displacement was 14.5 in for the SAP2000 nonlinear analysis using the LL average acceleration input, and 15.3 in for the SAP2000 analysis

using the UL average acceleration input. The numerical differences between the ACS SASSI and SAP2000 computed maximum displacements were less than 10%.

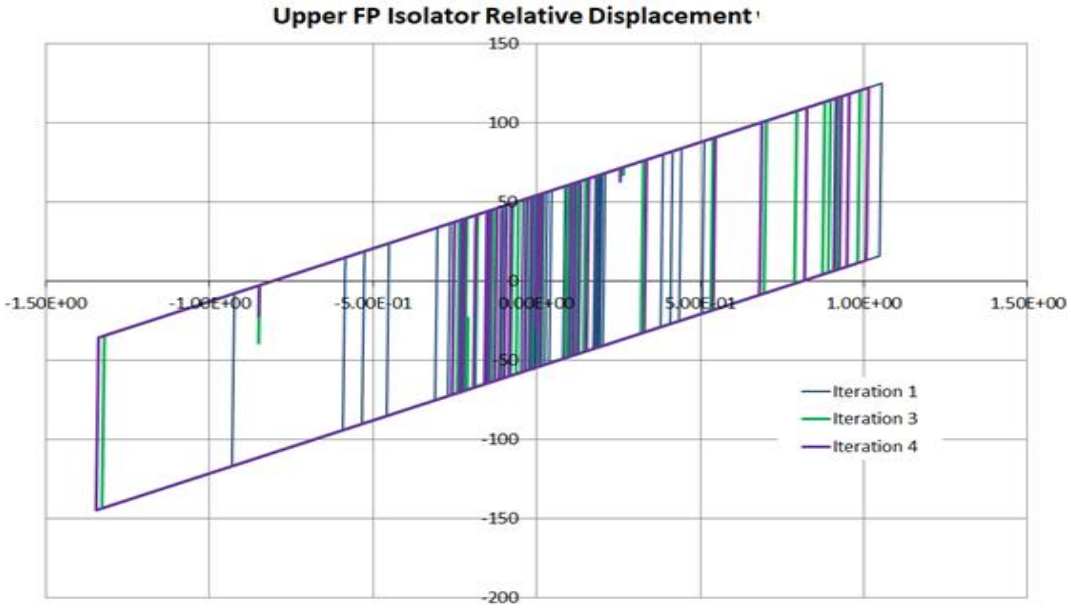

Figure 8. Type 2 FP Isolator Hysteretic Response for Vs=2000 fps Soil Case

. Table 1. Lateral Equivalent-Linear Isolator Properties Per SSI Analysis and ASCE 7-22 Equations

Isolators Location	Average Keff	Average Deff	Maximum Displacement	Isolators Location	Average Keff	Average Deff	Maximum Displacement
UL **SSI**	14.97 kip/in	22.2%	16.2 in	LL **SSI**	5.71 kip/in	22.2%	16.2 in
UL **ASCE 7**	13.81 kip/in	22.2%	18.5 in	LL **ASCE 7**	5.18 kip/in	22.2%	18.5 in
UL **% Diff**	8.4 %	0% Cut-off	12.4%	LL **% Diff**	10.4%	0% Cut-off	12.4%

Figure 9 shows the computed SIDRS in the X, Y and Z directions for the moat foundation at the two base-isolation support levels for Vs=5,000 fps soil. The SIDRS were computed by averaging the acceleration response spectra at the bottom of the pedestal supports for each of the two base-isolation levels.

The SIDRS at the two base-levels are different, which indicates that the foundation rigid body assumption is not an accurate assumption. This implies that significant elastic coupling forces and relative displacements occur between the two levels. The SIDRS concept introduced in the ASCE 4-16 Chapter 12, which is based on the foundation motion rigid body assumption, might not be directly applicable to the ARC-100 SMR Option 1 design solution with the two base-isolation levels at different embedment depths. The different motions at the two base-levels raises a question related to the significance of the effects of the inter-level relative displacements on the isolated superstructure response.

A rigorous Step 2 isolated-superstructure nonlinear analysis should consider the different base-level input motions as multiple support base excitations, including the two-level acceleration and the relative displacement time histories. The inter-level relative displacements may produce significant elastic coupling forces in both isolated-superstructure and the moat substructure.

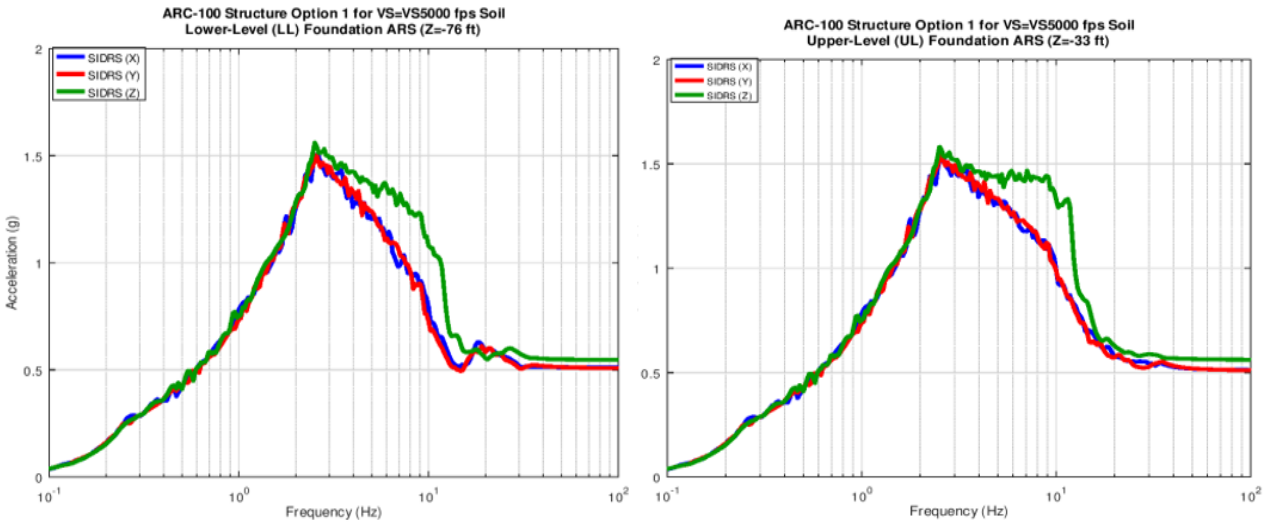

Figure 9 SIDRS Computed at Lower-Level (LL) and Upper Level (UL) for Vs=5,000 fps Soil

An additional intrinsic complexity of the two base-isolation level solution is the dynamic coupling which occurs between the moat foundation substructure and the isolated superstructure due to the LL isolators.

Figure 10 shows for the Vs = 2,000 soil, the SSI structural response accelerations (shown as deformed shape plots) on the embedded structure at two moments in time, 3.49 sec. and 5.86 sec. during the earthquake duration. The LL base motion appears visibly larger than the UL base motion at the 3.49 sec. time moment, and other time moments. This SSI motion amplification at the LL base is due to the dynamic coupling between the isolated superstructure and the moat foundation substructure responses. More specifically, the dynamic coupling is between the large amplitude vibration of the heavy hanged reactor vessel (RV) subsystem and the moat substructure. The RV subsystem is basically an inverse cantilever beam with a free moving end connected to the SMR foundation bottom basemat through the LL isolators.

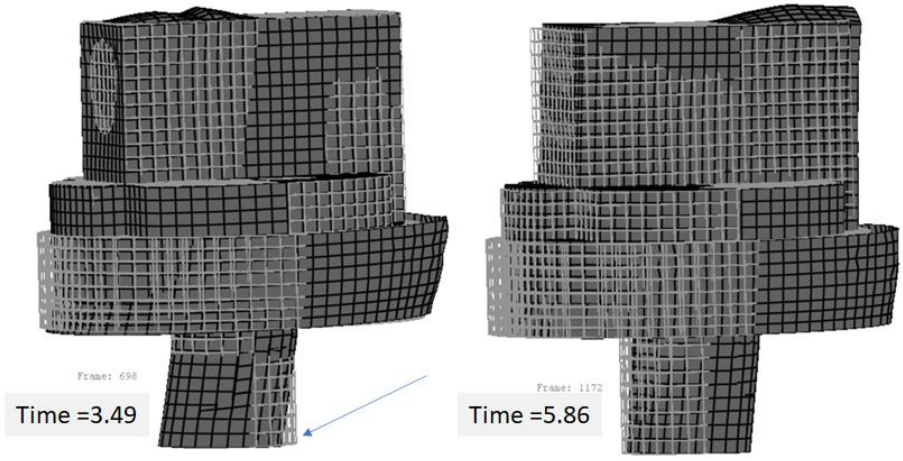

Figure 10. Instant SMR Structure Acceleration at Two Time Step Moments for Vs = 2,000 fps Soil

The largest dynamic coupling effects are in the vertical direction for which the LL FP isolators are not effective, as indicated by the difference between the two-level SIDRS amplitude in the vertical direction.

Figure 11 shows the effects of the two base-level differential motions on the transverse shear force QYZ (Q23) in the moat foundation substructure. It shows larger transverse shear forces in the UL basemat

at the connection with the moat cylindrical wall. The inter-level dynamic coupling will also affect the Step 2 nonlinear analysis results. Therefore, the application of the two-step cascaded SSI approach per the ASCE 4-16 standard recommendations based on the rigid foundation assumption, even if the envelope of the pedestal support accelerations is input for Step 2, could produce crude, overly or underly estimated, seismic responses of the isolated SMR superstructure.

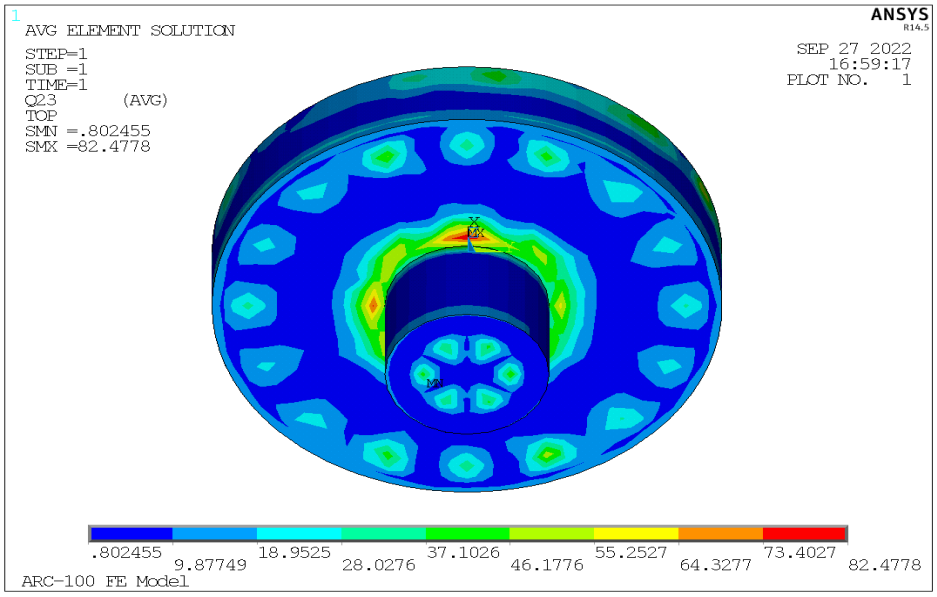

Figure 11 Transverse Shear Force QYZ (Q23) in Moat Foundation Substructure

Figures 12 and 13 show a comparison of the computed ISRS in the isolated superstructure for the three generic soils with Vs = 2,000 fps, Vs = 5,000 fps and Vs = 8,000 fps, respectively. It should be noted that the SSI effects are significant between the three soil SMR responses. It should be noted that that for the two soils with Vs = 2,000 and Vs = 5,000 fps, although the seismic input is defined by the same seismic RG1.60 input spectrum compatible surface ground accelerations, the ISRS results are significantly different. The ISRS peak amplitudes for the stiffer soil with Vs = 5,000 fps (red line) are substantially higher, up to 100% than the ISRS peak for the softer soil with Vs = 2,000 fps (blue line).

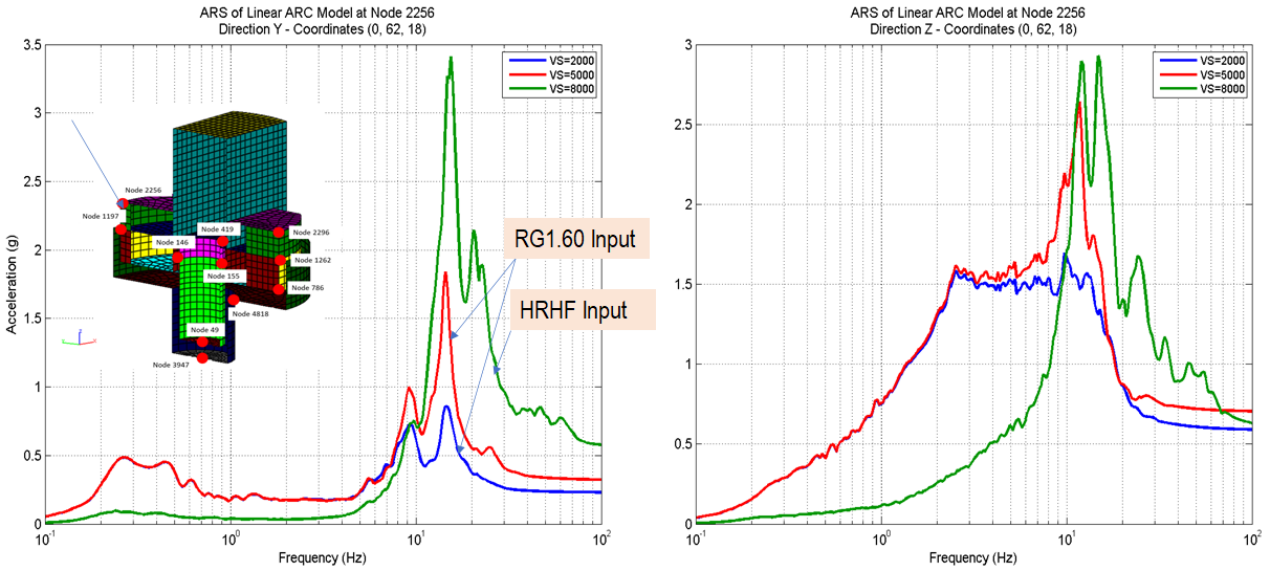

Figure 12. SMR ISRS at Low-Roof Edge in Y and Z Directions for Three Generic Site Conditions

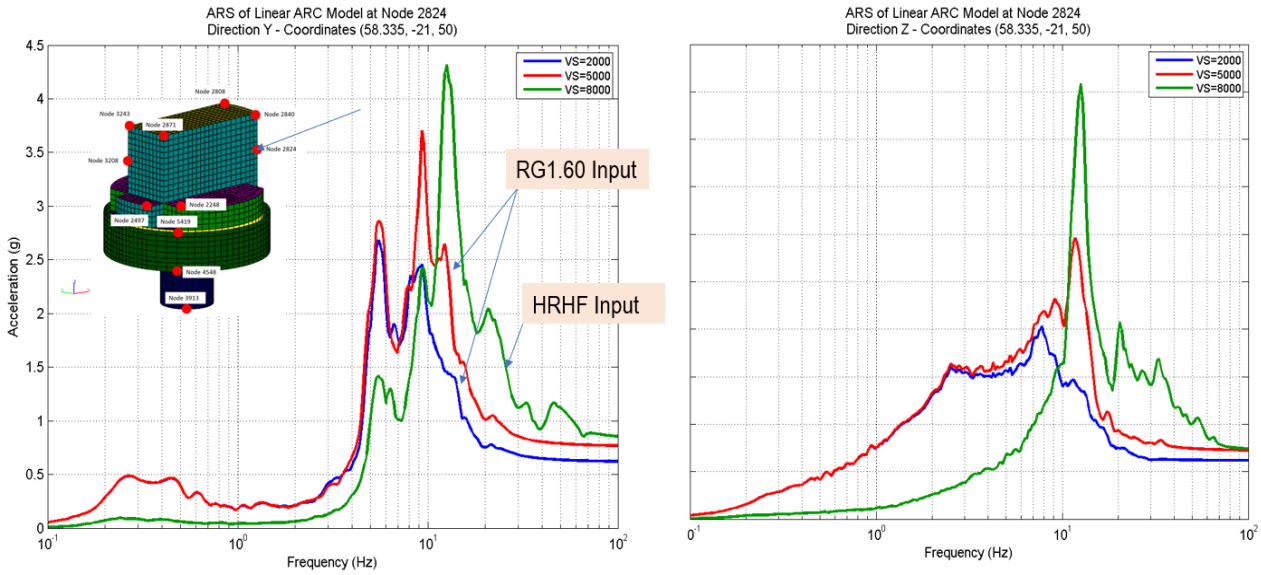

Figure 13. SMR ISRS at Higher-Elevation in Y and Z Directions for Three Generic Site Conditions

These ISRS differences due to SSI effects are larger for structural vibration modes in the 5-10 Hz frequency range. Only, for the very low-frequency isolator sliding mode @ 0.3 Hz, the two soil ISRS become identical. These comparative results clearly indicate that the SSI effects impact differently for different soils. It should be noted that these remarks are valid also for surface base-isolated RB complex buildings (Ghiocel, 2017). Only if the isolated structures are assumed to behave exactly as SDOF oscillators, having only a single, very low-frequency sliding mode, the seismic SSI effects will be negligible. The neglect of SSI effects could impact severely on the accuracy of the computed ISRS as shown in Figures 12 and 13.

An important influential factor that was not considered so far in the study, but which could severely amplify the base-isolated structure ISRS responses, is the effect of the seismic motion spatial variations, including motion incoherency and wave passage effects. As shown by some recent studies, the seismic motion incoherency could significantly increase the ISRS amplitudes in the 5-12 Hz frequency range (Bulut et al., 2015, Ghiocel, 2019, Ghiocel et al., 2022). As a result of the soil differential displacements induced by soil motion spatial variation, the isolator axial forces could severely increase. Ahmad et al. showed that the motion incoherency effects resulted in a severe increase of isolator fragilities which are 1.9-2.5 times larger than fragilities computed for coherent input motions (Ahmad et al., 2015)

5. CONCLUDING REMARKS

The paper addresses the seismic SSI analysis of the deeply embedded, base-isolated ARC-100 SMR structure as a part of a conceptual design research study. The early research study included two SMR design base-isolation solutions: 1) An initial, Option 1 solution with two base-isolation levels, and 2) An improved, Option 2 solution with a single base-isolation level. Three generic site-specific conditions were considered. The multistep SSI analysis methodology recommended in the ASCE 4-16 Section 12 is applied.

The paper focuses on the understanding of the complexity of the seismic SSI behaviour of the Option 1 design solution with two base-isolation levels. It is shown that for this investigated solution, there are some modelling difficulties created by the fact that the SSI motions computed at the two base-isolation levels are slightly different, which indicates that the foundation rigid body assumption and the application of the cascaded multistep SSI approach per ASCE 4-16 are not fully accurate.

The seismic SSI analysis results performed for the base-isolated SMR for different soils show significant SSI effects on the ISRS, even if the same seismic ground surface input is used, as shown herein for Vs = 2000 fps and Vs = 5,000 fps soils. This important practical aspect is sometimes overlooked.

The Option 2 design solution that appeared simpler, more robust, was finally considered for the ARC-100 SMR base-isolation design solution.

6. REFERENCES

ACS SASSI NQA Version 4.3.5 (2022) *An Advanced Computational Software for 3D Dynamic Analysis Including Soil-Structure Interaction*, GP Technologies, Inc., User Manuals, Revision 8, Pittsford, New York

Ahmad, K., Sayed, M.A. and Kim, D. (2015). *Seismic Fragility of Base-Isolated Nuclear Power Plant Structures Considering Spatially Varying Ground Motions*, SMIRT23 Conference, Division XII, Manchester, UK, August 10-14

ASCE 4-16 (2017) and ASCE 4-23 draft (dated 8/20/2021), *Seismic Analysis of Safety-Related Nuclear Structures,* Chapters 2, 5 and 12, ASCE/SEI

ASCE 43-19 (2020*) Seismic Design Criteria for Structures, Systems, and Components in Nuclear Facilities*, ASCE/SEI

ASCE 7-22 (2022), *Minimum Design Loads and Associated Criteria for Buildings and Other Structures*, Chapter 17, ASCE/SEI

Bulut, Y., Weber, F., Erbay, O., Paroli, L., Huber, P., Distl, J., Braun, C. and Ghiocel, D (2017). *Seismic SSI Effects on Design of Curved Sliders for Base Isolation and Recentering Capability of Rectangular Shearwall Structures*, SMIRT24 Conference, Division V, BEXCO, Busan, Korea, August 20-25

Ghiocel, D.M. (2019). *Probabilistic Seismic SSI Analysis Sensitivity Studies for Base-Isolated Nuclear Structures Subjected to Coherent and Incoherent Motions*, SMIRT25 Conference, Division III, Charlotte, NC, August 4-9

Ghiocel, D.M. (2022). *A Study on Seismic SSI Analysis of A Base-Isolated Storage Structure Founded on Form Soil*, SMIRT26 Conference, Special Session on Seismic Isolation, Berlin/Postdam Germany, July 10-15

Nie, J. (2019), *Assessment of Artificial Acceleration Time History Guidance on SRP Section 3.7.1. "Seismic Design Parameters",* USNRC RIL-2019-01, NRC Office of Nuclear Research

NUREG/CR-7253 (2019) *Technical Considerations for Seismic Isolation of Nuclear Facilities,* A.M. Kammerer, A.S. Whittaker, and M.C. Constantinou

NUREG/CR-7254 (2019) Seismic Isolation of Nuclear Power Plants Using Sliding Bearings, M. Kumar, A. Whittaker, M. Constantinou

NUREG/CR 07255 (2019) *Seismic Isolation of Nuclear Power Plants using Elastomeric Bearings,* M. Kumar, A. Whittaker, M. Constantinou